Chapter 9
The Antenna Research System Task

The Antenna Research System Task (ARST) was a study and technology demonstration to explore the engineering aspects of combining transmitted pulses in position, time, and phase from independent radar systems [1], as well as to determine the applicability of using a beam-waveguide (BWG) system for high-power applications in large ground station antennas [2]. Toward this objective, the Jet Propulsion Laboratory (JPL) designed, constructed, and tested a Technology Demonstration Facility (TDF), consisting of two 34-m-diameter BWG antennas (see Fig. 9-1) and associated subsystems.

Fig. 9-1. The ARST antennas.

JPL's interest in uplink arraying and high-power technologies stems from its responsibilities in managing the Deep Space Network (DSN) for the National Aeronautics and Space Administration (NASA). Combining signals from two or more antennas in an uplink array has possible application in emergencies such as the loss of a high-power DSN transmitter or the loss of a high-gain antenna on a spacecraft. It would also be required to provide an uplink capability for an array of small reflectors.

In a BWG system, the feed horn and support equipment are placed in a stationary room below the antenna, and the energy is guided from the feed horn to the subreflector using a system of reflecting mirrors. Thus, there is no limit on the size of the transmitter system and it can be placed directly behind the feed, minimizing waveguide losses. One purpose of the TDF was to design a BWG system that would not degrade either the peak or average power handling capability of a large ground station antenna beyond the limitations imposed by either the feed or the dual-reflector configuration.

A 34-m main diameter was chosen for the study because JPL already had experience with conventional BWG antennas of the same size. The high-power design featured a transmit-only, four-port high-gain feed horn as input to a BWG system consisting of a single parabolic mirror and three flat plates. By using a single parabolic mirror, there is no further concentration of the field and, therefore, the highest field concentration is no greater than that caused by the feed horn itself. The feed horn is linearly polarized, and a duplexing reflector is used to reflect the orthogonal polarization into the receive feed. A rotatable dual polarizer provides for arbitrary transmit polarization. The dual-reflector system is shaped to provide uniform illumination over the main reflector and, therefore, maximum gain for the given size aperture. Unfortunately, due to funding limitations and unavailability of a suitable transmitter, the ARST antennas were never tested at high power. However, since significant effort went into the design and fabrication of the transmit feed horn, and the BWG demonstrated a design capable of maximum power, the details of the design and testing are included in this chapter.

Using a monopulse feed in the BWG receive path, along with a low-power transmitter, the ARST uplink arraying experiments were performed by tracking orbiting debris or satellites using the TDF's two antennas, each transmitting pulses to the objects. The TDF then measured the phase for each returned pulse and adjusted the phase and timing of one transmitter (the "slave") so that the next pulses would combine coherently at the object. These experiments permitted JPL to evaluate, characterize, and demonstrate the following:

- The ability of large antennas to track objects with sufficient accuracy to support timing and phase synchronization under various environmental conditions

- The ability to control phase and timing of pulses transmitted from two antennas to an object in order to maintain radio frequency (RF) carrier phase within calibration limits while tracking the object
- The significance of atmospheric effects
- The measurement accuracy of the average phase difference between signals reflected from complex-shaped objects as a function of signal-to-noise ratio (SNR) and object scintillation.

Upon completion of the uplink demonstration, the antennas were to be retrofitted with standard DSN equipment and used as additional resources for the DSN to track spacecraft. An S-band feed system and associated equipment were installed in one of the two antennas (Deep Space Station 27 [DSS-27]); the system is currently used to track high Earth-orbiting spacecraft.

9.1 Design of the Beam-Waveguide System

The more conventional BWG designs discussed in Chapters 7 and 8 use four mirrors to direct the feed-horn radiation around the two axes of rotation and to the subreflector. These designs use two curved mirrors, either ellipsoids or paraboloids, and two flat mirrors. This four-mirror system images the feed horn at a location near the apex of the main reflector. Such a configuration results in a dual reflector that is nearly a Cassegrain system, with the standard hyperbola-parabola configuration modified slightly (shaped) in order to provide essentially uniform illumination over the main reflector, thus providing nearly optimum gain.

For high power, the refocusing of the feed-system energy near the main reflector has two distinct disadvantages. First, since the peak field point is generally at or in front of the feed horn itself, the peak power point is imaged in front of the main reflector. If the peak field point can be contained within the BWG system, it is possible to fill the BWG tube with a gas to enhance the peak-power handling capability of the system. Also, when the energy is reflected from a surface such as a BWG mirror, there is a 6-dB enhancement of the power near the reflector, since the incident and reflected field add coherently near the reflection point. It is thus important to have the energy near the mirrors at least 6 dB below the peak point in order to prevent the mirrors from degrading the power handling capability of the system. This is difficult to do if the energy is refocused in the BWG system. For these reasons, an unconventional design [2,3] was chosen for the BWG optics. Figure 9-2 shows the detailed dimensions for the antennas.

For this design, only one curved mirror—a paraboloid—is used, along with three flat mirrors. The radiation from the feed horn is allowed to spread to the

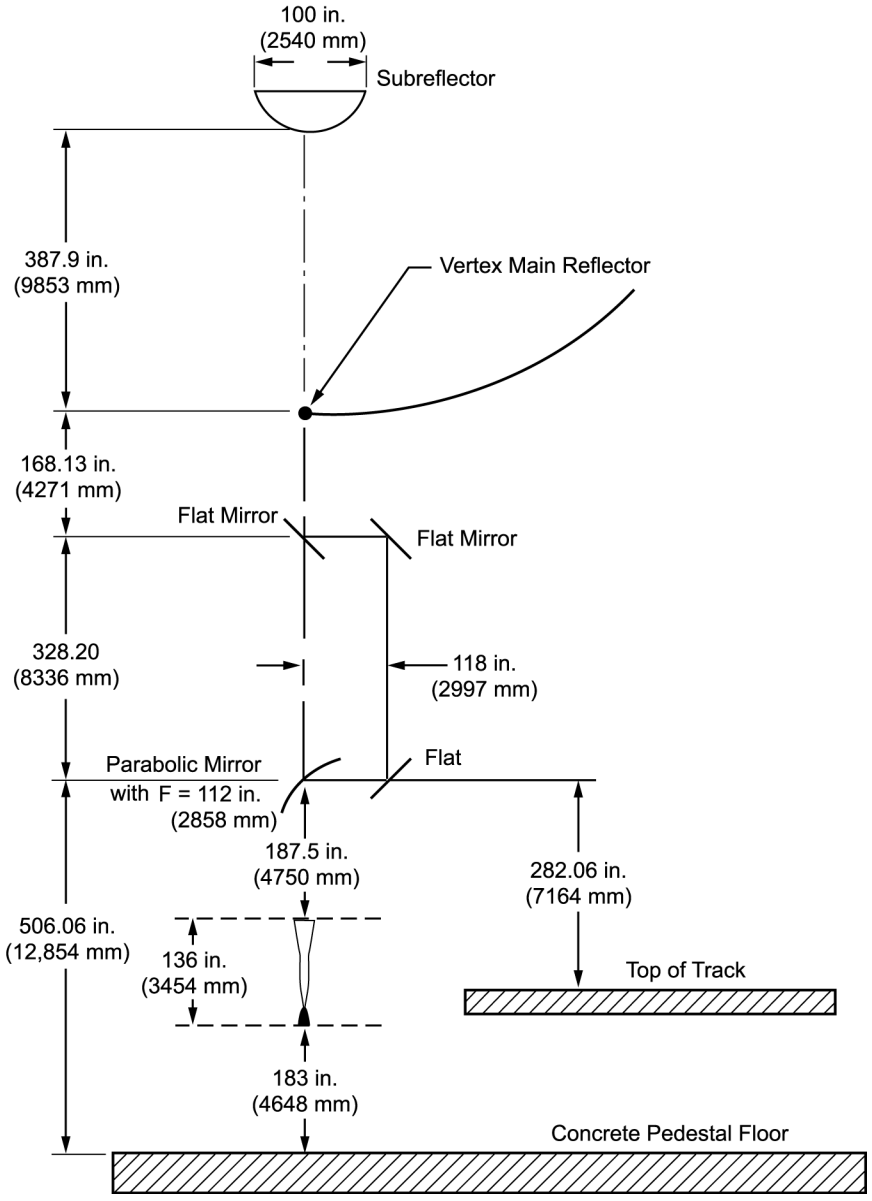

Fig. 9-2. Geometry of the ARST antenna.

paraboloid, where it is focused to a point at infinity. That is, after reflection, a collimated beam exists that is directed to the subreflector by the three flat reflectors. The energy is thus spread over the 2.743-m diameter of the BWG tube. Due to diffraction, the beam reflected by the paraboloid does not begin to spread significantly until it exits through the main reflector. At that point, addi-

tional spreading occurs in the region between the main reflector and the subreflector. Since a collimated beam exists beyond the first mirror, this antenna is closely related to a near-field Cassegrain design, where the feed system is defined to include both the feed horn and a parabolic mirror.

Both the main reflector and the subreflector are nominally paraboloids, with dual-reflector shaping used to increase the illumination efficiency on the main reflector by compensating for the amplitude taper of the feed radiation pattern. The design of the dual-shaped antenna is based upon geometrical optics, with the shape of the subreflector chosen to provide for uniform amplitude illumination of the main reflector, given the distribution of the radiation striking the subreflector. The curvature of the main reflector is then modified slightly from that of the parent paraboloid to compensate for any phase errors introduced by the subreflector shaping. In the present design, the deviation of the main reflector surface from that of the parent paraboloid is less than 2.5 cm at every point on the 34-m-diameter surface. Although the design of the surfaces is based on geometrical optics, the final design is then analyzed using physical optics, thus including diffraction effects, in order to predict the overall performance accurately.

Figure 9-3 shows the predicted far-field patterns of the overall antenna. The calculated gain (at the center frequency of 7.2 GHz) is 67.67 dB. This

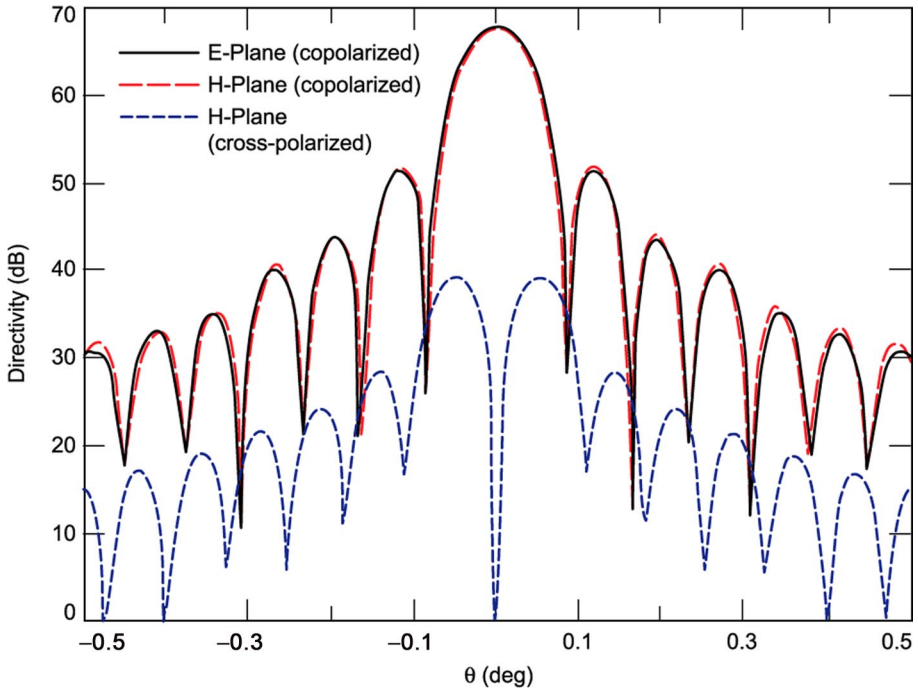

Fig. 9-3. Far-field patterns of the overall antenna.

number is based upon a purely theoretical calculation, and the following effects are neglected: polarizer and duplexing grid effects on the feed-horn radiation pattern, shroud effects, root-mean-square (rms) surface accuracy of all mirrors, subreflector and main reflector, quadripod blockage, and feed-horn loss. The specification for surface accuracy is 0.20-mm rms for the subreflector and BWG mirrors, and 0.89-mm rms for the main reflector at the rigging angle. If we define antenna efficiency as the actual gain for the antenna as designed divided by the maximum theoretical gain for a 34-m-diameter circular aperture at 7.2 GHz, we may estimate the following efficiency for the present design: the calculated gain quoted above represents an RF efficiency of 91 percent. The efficiency due to main reflector surface accuracy is calculated to be 93.1 percent and quadripod blockage gives an efficiency of 89.2 percent, for an overall efficiency of 75.6 percent. Including the other factors—BWG mirrors, polarizer, duplexing grid, ohmic loss from the mirrors, voltage standing-wave ratio (VSWR) effects, and BWG mirror alignments—gives an efficiency referenced to the feed input of 73 percent. The antenna was never actually measured from the transmit feed port, but rather by using a monopulse feed in the receive system path [4]. The feed efficiency budget is shown in Table 9-1 and shows a predicted efficiency of 68 percent. The measured efficiency referenced to the feed input was 65 percent for the east and 64 percent for the west antenna. The noise temperature budget, shown in Table 9-2, was 26 K. The measured noise temperature was 21 K.

9.2 Design of the Transmit Feed Horn

The basic requirements of the primary transmit feed horn were

- Sufficient gain to minimize spillover past the first parabola in the BWG system
- The peak field point positioned inside the feed horn so that a vacuum system for the feed would result in maximum power handling capability
- Equal E- and H-plane patterns to maximize efficiency in the dual-reflector system
- Arbitrary polarization capability
- Placement far enough from the first mirror so that the energy level at the first mirror was 6 dB below the peak level between the feed and the mirror
- A window design for the feed system mechanically capable of holding a vacuum with minimum radio frequency (RF) loss
- Multiple input ports to enable combining a number of transmitters.

Table 9-1. The ARST 34-m BWG antenna receive (monopulse) feed efficiency budget.

Element	Sum Pattern at 7.2 GHz	Notes
Main reflector		
Ohmic loss	0.99957	Calculated
Panel leak	0.99992	Calculated from DSS-13 model
Gap leak	0.9982	Calculated from DSS-13 model
(main reflector + subreflector) rms	0.94509	Calculated (rms = 0.79 mm)
Subreflector ohmic loss	0.99957	Calculated
4 BWG mirrors		
Ohmic loss	0.99829	Calculated
rms	0.99251	Calculated (rms = 0.20 mm)
Hyperboloid mirror		
Ohmic loss	0.99957	Calculated
rms	0.99625	Calculated (rms = 0.20 mm)
BWG/Cassegrain VSWR	0.999	Estimated
Polarizer		
Ohmic loss	0.998	Estimated
Reflection	0.998	Estimated
Duplexing grid		
Ohmic loss	0.999	Estimated
Reflection	0.995	Estimated
Feed-support blockage	0.8946	Estimated
Pointing squint	0.9696	0.008-deg pointing loss
BWG mirror alignments	0.9994	Estimated
Subtotal	0.79732	
Physical optics efficiency	0.85114 67.48 dB	Physical optics analysis
Total at feed aperture	0.6786 68.18 dB = 100%	

All of the above requirements are satisfied using a four-input port, linearly polarized, square, multiflare feed [5] with a double output window, as shown in Fig. 9-4. Arbitrary polarization is accomplished using dual-rotary vane polarizers described in Section 9.4. The various flare angles in the design are used to achieve equal E- and H-plane patterns and a tapered amplitude distribution at the output, which puts the peak energy point inside the feed. This is demon-

Table 9-2. The ARST 34-m BWG antenna receive (monopulse) feed noise-temperature budget.

Element	Sum Pattern at 7.2 GHz	Notes
Cosmic background	2.50	Effective blackbody
Main reflector		
Ohmic loss	0.13	Calculated
Panel leak	0.02	DSS-13 model
Gap leak	0.50	DSS-13 model
Rear spill	0.55	T_{eff} = 240 K
Subreflector ohmic loss	0.13	Calculated
4 BWG mirrors		
Ohmic loss	0.50	Calculated
Hyperboloid mirror		
Ohmic loss	0.13	Calculated
Spill	6.62	T_{eff} = 240 K
Polarizer	1.16	Estimated
Duplexing grid	1.74	Estimated
Atmosphere	2.17	Goldstone (average clear)
F_1 fields/forward spill/ground	0.02	T_{eff} = 5 K
Spillover from 4 upper BWG mirrors	7.15	T_{eff} = 240 K
Quadripod scatter	2.70	Estimated (DSS-24)
Subtotal (K)	26.02	Noise at feed aperture

strated in Fig. 9-5, which plots the relative power density on axis as a function of distance from the feed horn. Figure 9-5 also shows that the energy level at the distance of the first mirror (187 in. [4.75 m]) is 12 dB below the peak value between the feed and mirror.

The design of the window system for this feed horn is a key issue. A dual-quartz window is used. Figure 9-6 shows the geometry of the window system sitting on top of the ARST primary feed aperture. Each window is approximately one-half wavelength thick at the center frequency of operation. The spacing between the windows is chosen to minimize reflections for some band of frequencies. The calculated reflection properties for the window section are shown in Fig. 9-7, along with results for a single half-wave-thick quartz window. Specifications for typical transmitters indicate that the VSWR for the entire feed assembly should be less than 1.1 over a ± 5 percent frequency band. As can be seen from Fig. 9-7, a single half-wave-thick quartz window fails to meet the requirement, particularly since additional factors such as combiner

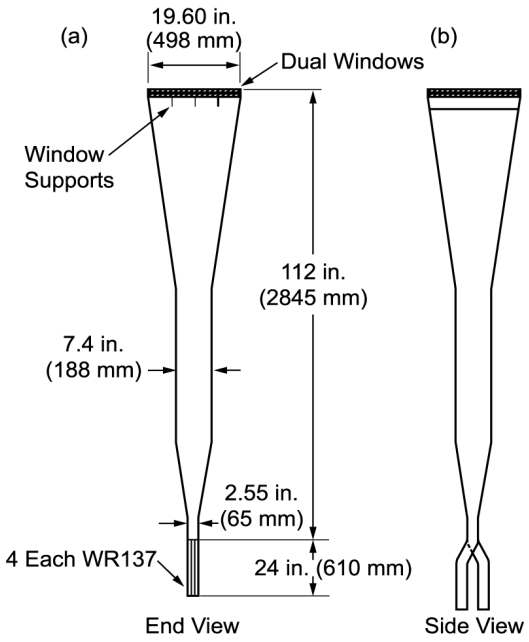

Fig. 9-4. Important dimensions of the feed horn: (a) end view and (b) side view.

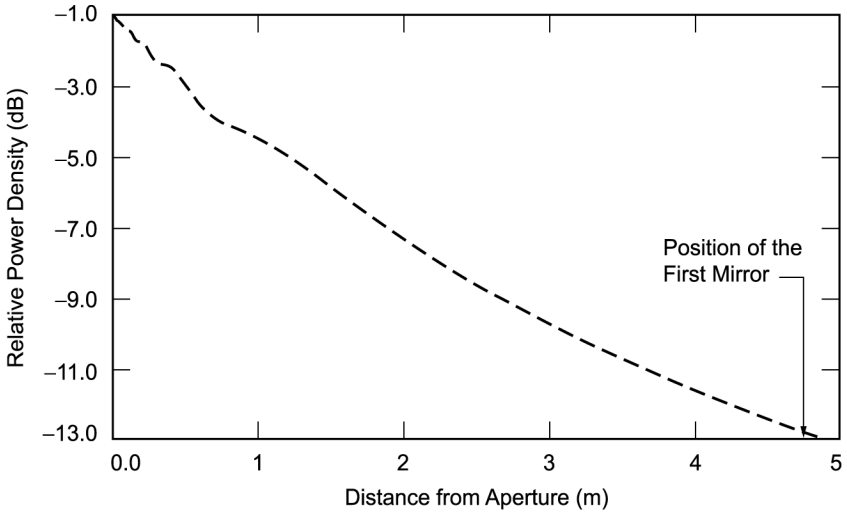

Fig. 9-5. Relative power density on axis as a function of the distance from the feed horn.

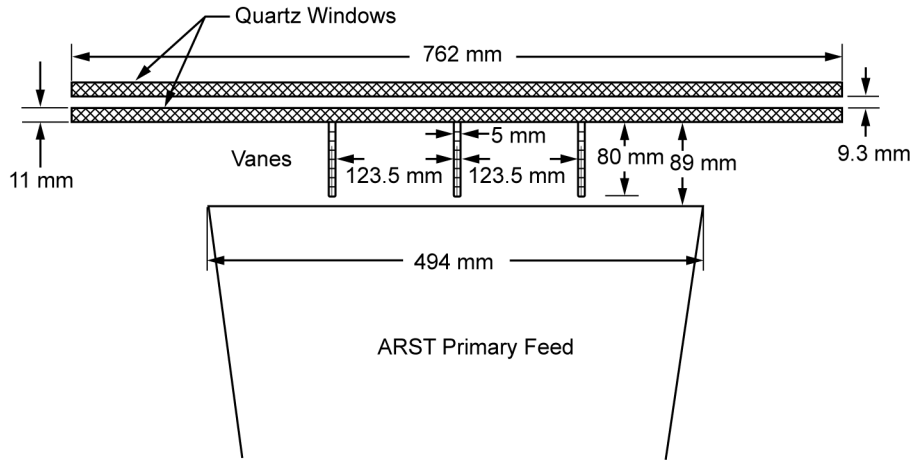

Fig. 9-6. Geometry of the window system.

design is able to meet the requirement. This is accomplished by choosing the window thickness so that both windows are perfectly matched at one frequency, and choosing the window spacing so that reflections from the two windows cancel at a second frequency. For frequencies between these values a small reflection will exist, as is shown in the figure, but sufficient bandwidth is available from the dual-quartz window design to meet the VSWR requirement.

Another important property of the window is its mechanical integrity; a 20-in. (508-mm)-diameter window would not be capable of supporting a vacuum. The solution to the window problem was found by using the fact that the radiation inside the feed horn is linearly polarized. This allows the placement of

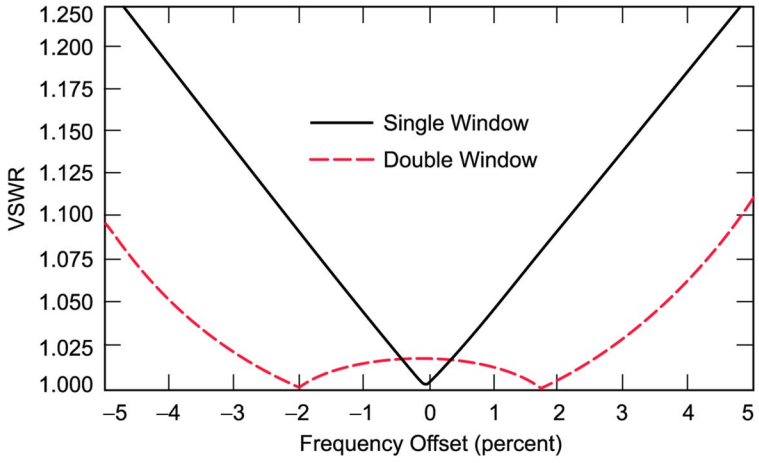

Fig. 9-7. Calculated reflection from single and double windows as a function of frequency.

support fins under the window that are orthogonal to the electric field. With the help of a structural engineer, a solution giving minimum blockage was found consisting of three support fins. A finite element analysis of the entire structure was performed to verify the structural integrity of the window, and RF calculations indicate that the VSWR requirements placed on the feed horn by the transmitter can still be met.

This design combines high efficiency with a realizable window design and is, therefore, the design of choice. All of the antenna optics have been designed around this feed horn, and RF testing of a scale model was completed. Figure 9-8 shows a comparison of the calculated and measured radiation patterns for the scale-model feed horn. A picture of the scale-model feed horn is shown in Fig. 9-9 showing the fins that support the window. The measured pattern was for a scale-model feed horn at 31.4 GHz, and the theoretical pattern was computed for the design shown in Fig. 9-4 at 7.2 GHz. The transmit feed horn has four input ports so that four transmitters could be combined in the feed horn. A picture of the four-port coupler is shown in Fig. 9-10. Details of the full-scale primary feed development can be found in [6].

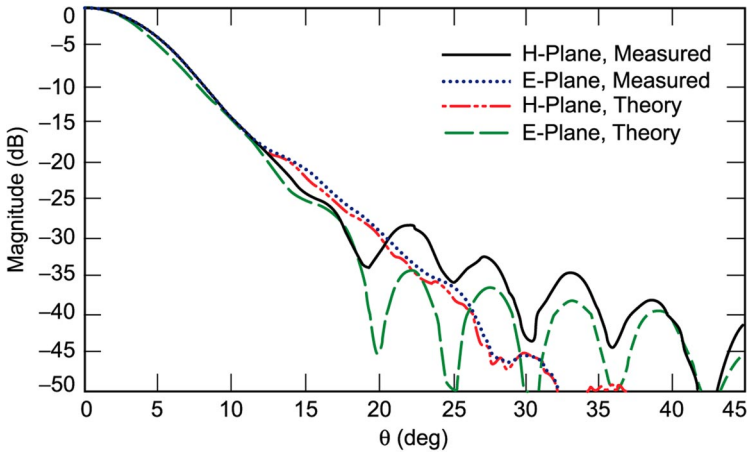

Fig. 9-8. Comparison of calculated and measured radiation patterns for the scale-model feed horn.

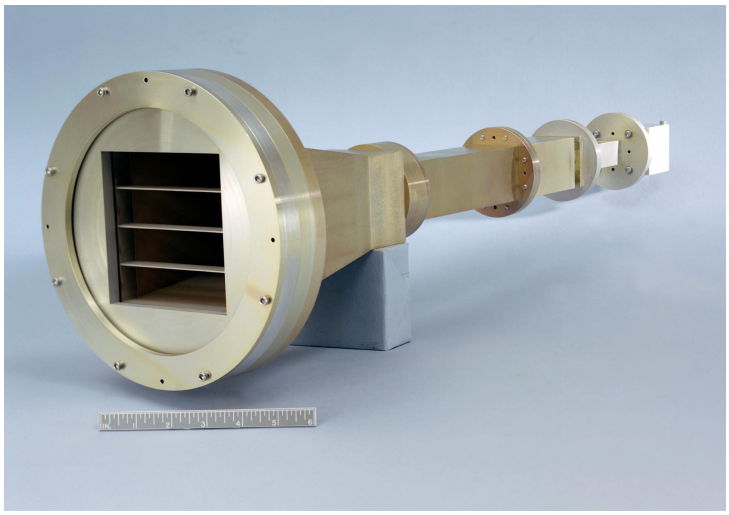

Fig. 9-9. Scale model of the ARST primary feed.

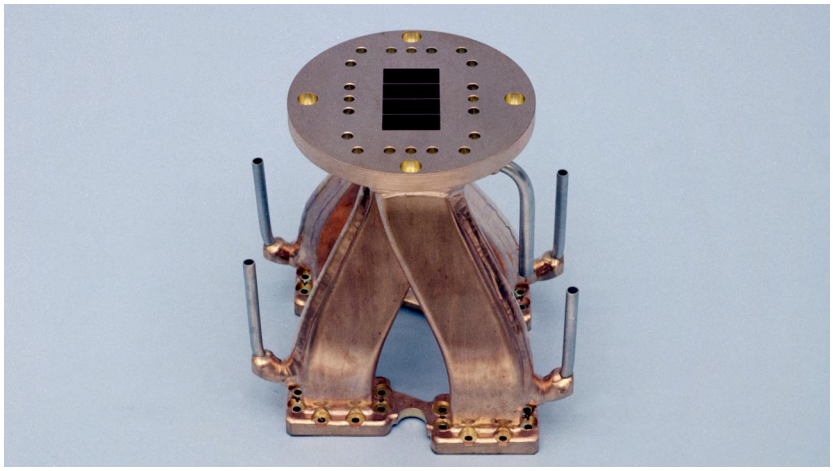

Fig. 9-10. Primary feed-horn combiner.

9.3 Receive-System Design

The receive system design is shown in Fig. 9-11. It consists of a duplexing grid that reflects the orthogonal polarization towards a curved mirror that is designed to be used with a monopulse receive feed horn. The curved mirror is a hyperbola with focal points at the receive feed horn and the reflected image of the parabola focal point. The monopulse receive feed horn is a scaled version of

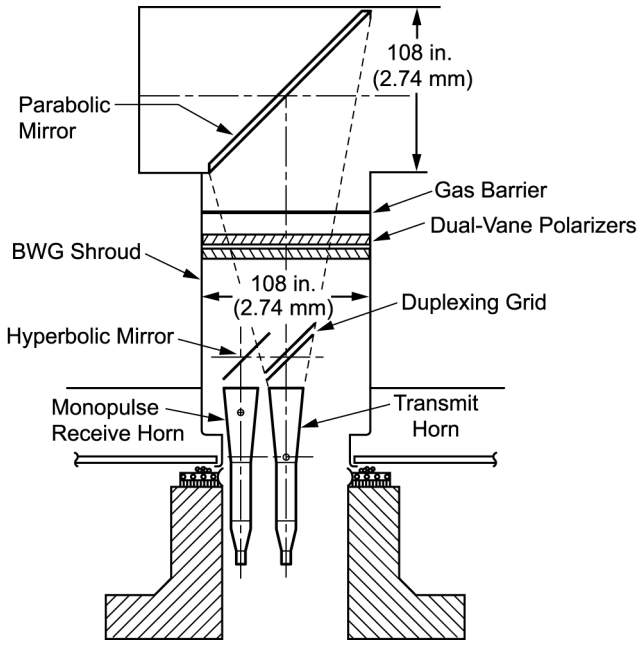

Fig. 9-11. Schematic diagram of the total feed system.

the Haystack feed horn [7]. Preliminary calculations were carried out in order to verify that acceptable monopulse performance—that is, tracking to within 1/20 of a beamwidth—could be obtained on the 34-m antenna.

The duplexing grid is a plane reflector that is formed by a series of thin metal strips. If the strips are spaced closer than one-half wavelength, a signal that is polarized parallel to the strips (in this case the received signal) is reflected, while one perpendicular to the strips (in this case the signal from the transmit feed horn) is transmitted. In order to achieve minimal reflection in the perpendicular mode, the dimensions of the strips must be adjusted for the frequency band of interest. Figure 9-12 shows the computed reflection from the grid in the perpendicular mode over the band of interest. It can be seen that less than 0.1 percent of the incident energy is reflected over the band of interest. It should be noted that this reflected energy does not reflect back into the feed horn, but rather is reflected off the grid to the right (see Fig. 9-11), where it will either be absorbed or reflected again. Therefore, the grid should have minimum impact on the VSWR seen by the transmit feed horn, and essentially no effect on the transmitted energy. A Ka-band scale model of the ARST primary feed window system and duplexing grid were built and RF measurements made in the JPL BWG test facility [8]. The setup is shown in Figs. 9-13 and 9-14. Notice the duplexing grid attached to the top of the feed. The measured patterns (including window and grid) in Fig. 9-15 were compared to the theoretical pat-

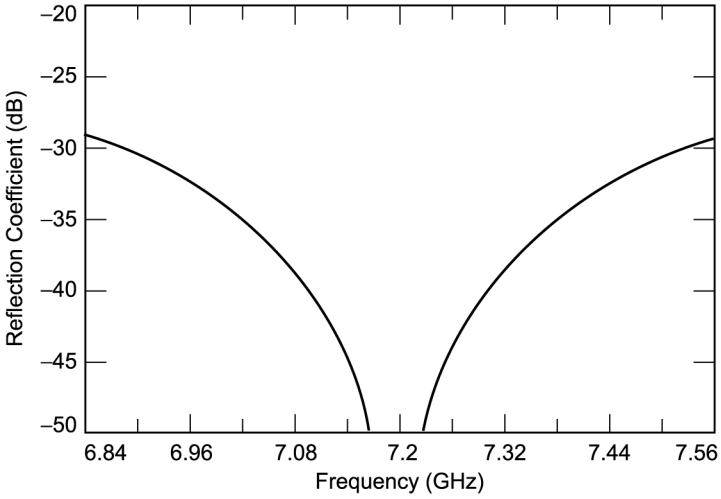

Fig. 9-12. Calculated reflection from the duplexing grid in the perpendicular mode.

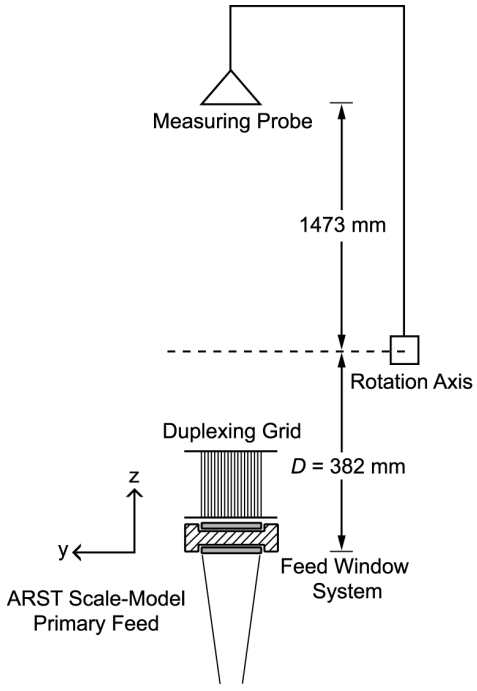

Fig. 9-13. Measurement setup of the scale model.

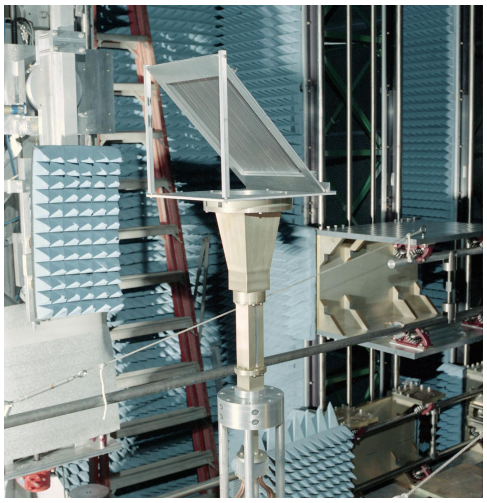

Fig. 9-14. RF testing of the scale-model feed.

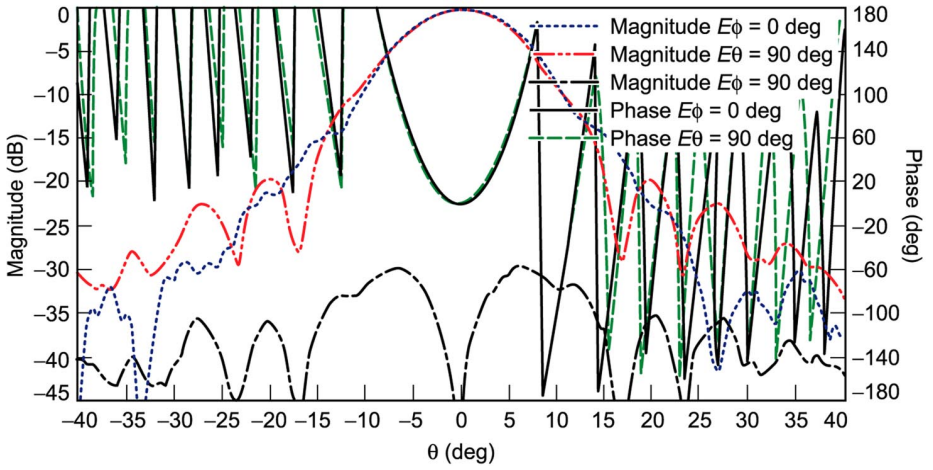

Fig. 9-15. Measured pattern of the scale model at Ka-band.

terns of Fig. 9-16, which did not include the effects of the window or grid. The difference between the measured and predicted radiation patterns is shown in Fig. 9-17.

The agreement of the measured and computed patterns in the range [–10 deg, +10 deg] is within ±1 dB for the amplitude and within ± 20 deg for the phase. This means that the effects of the window system and the duplexing grid on the ARST primary-feed radiation pattern at the center frequency of 7.2 GHz are minimal.

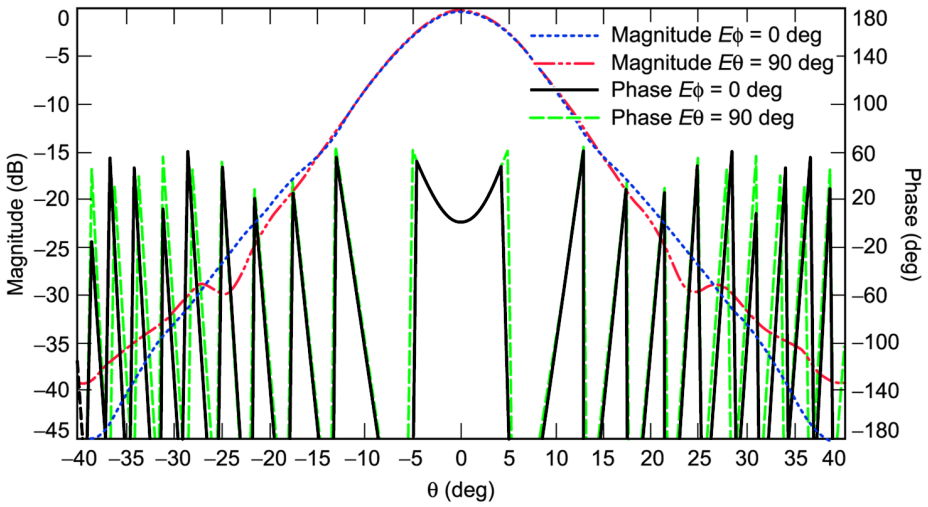

Fig. 9-16. Theoretical radiation patterns at X-band.

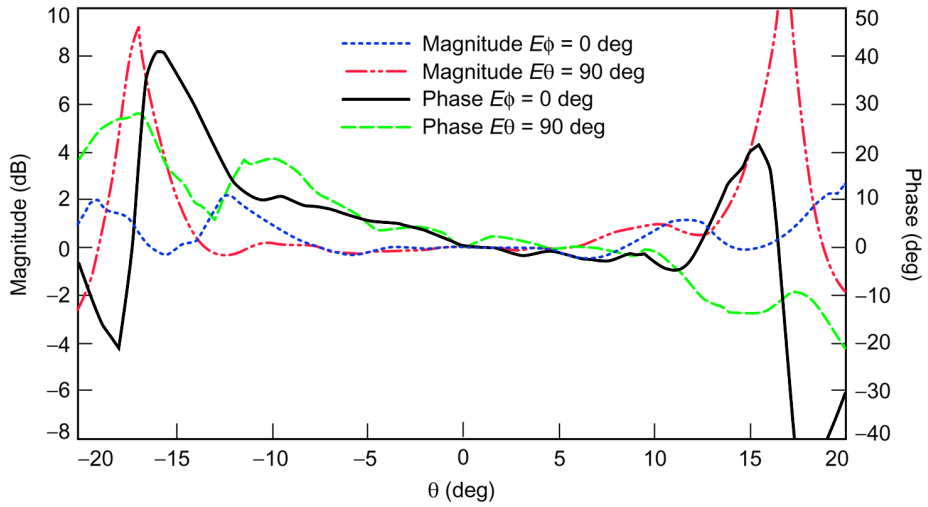

Fig. 9-17. Difference between measured and computed radiation patterns.

9.4 Dual-Vane Polarizers

A broadband venetian blind dual-vane polarizer was designed to be used in the ARST 34-m BWG antenna [9]. At first, a single-vane polarizer design was considered. However, when a prototype was built and tested in the JPL antenna range, it was discovered that the radiation pattern was distorted for the E-perpendicular mode in the cut made perpendicular to the vanes. Upon further investigation, it was determined that the cause of the problem was the extreme sensitivity of the single-vane polarizer to off-axis illumination, which created a high reflection at the center design frequency.

It was at that point that the polarizer was broken up into two sets of vanes separated by some distance. The space between the sets of vanes was selected so that the reflections from the second set would cancel those from the first one. Also, each set of vanes was designed to create a 45-deg phase shift in order to make the overall change equal to 90 deg. Figure 9-18 shows the design dimensions of the venetian blind dual-vane polarizer.

The calculated return loss for the E-parallel and E-perpendicular modes of the dual-vane polarizer is shown in Fig. 9-19. This figure shows that the worst reflection from this polarizer is close to –25 dB at the edge of the 5 percent frequency band.

Figure 9-20 shows a comparison of two measured radiation patterns of a test feed horn. One pattern is of the feed horn by itself and the other one is with the polarizer. The patterns are those for the E-field mode in the cut perpendicu-

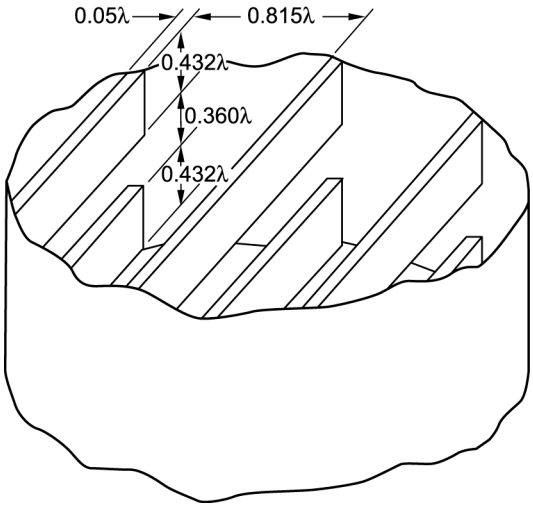

Fig. 9-18. Venetian blind dual-vane polarizer.

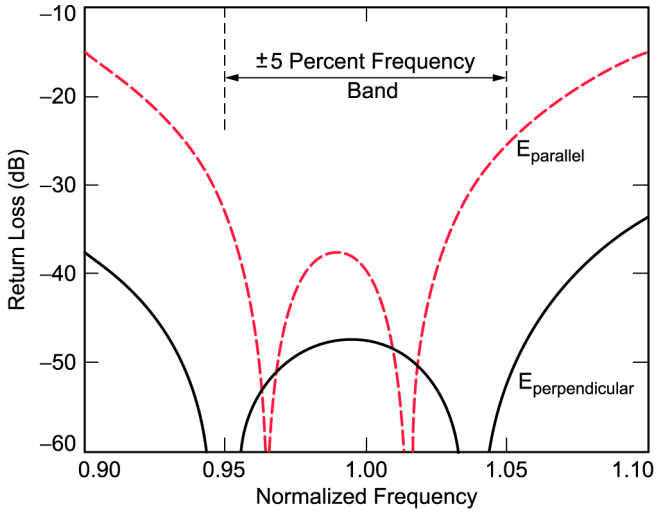

Fig. 9-19. Return loss of the dual-vane polarizer.

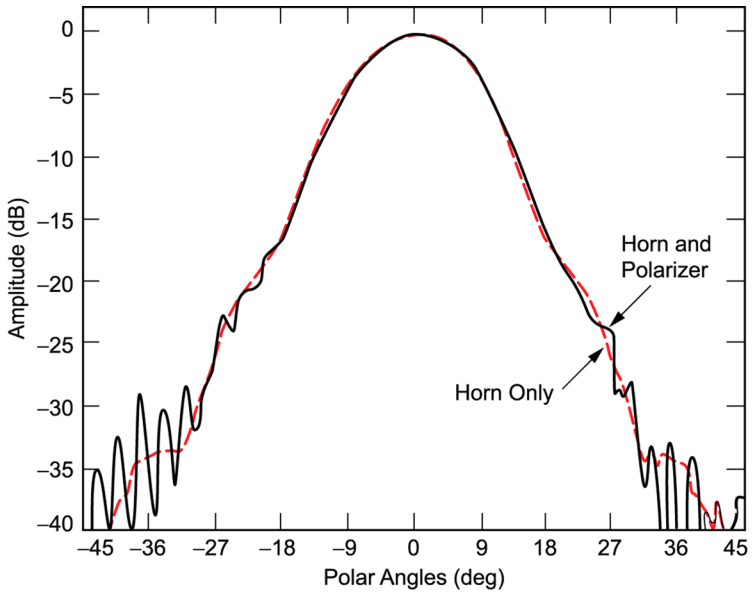

Fig. 9-20. Effects of the dual-vane polarizer on the horn pattern.

lar to the vanes. It was this mode that showed noticeable pattern deformation when a single-vane polarizer was used. As can be seen, the dual-vane polarizer has very little effect on the transmit signal of the illuminating feed horn.

Figure 9-21 details the three main modes of operation of the dual-vane polarizer system. In the first two modes, the first polarizer is set so the vanes are perpendicular to the E-field, and the second polarizer is oriented to produce right-hand circular polarization (RCP) for the first mode or left-hand circular polarization (LCP) for the second mode. In the third mode, the first polarizer is set at 45 deg to the E-field from the feed horn, thus producing RCP between the two polarizers. The second polarizer accepts this RCP and outputs a linear signal at 45 deg to the orientation of the vanes. In the figure, this is shown as being in the y-direction, but linear polarization can be produced at any angle by rotation of the second polarizer.

9.5 Uplink Arraying

An uplink arraying experiment was performed using a monopulse feed and a low-power transmitter in the receive system path and is well documented in [1]. Since the uplink array experiment is primarily a system demonstration, and the main focus of this book is primarily on the RF design and performance of the antennas, only the abstract of [1] is presented here. The report describes the

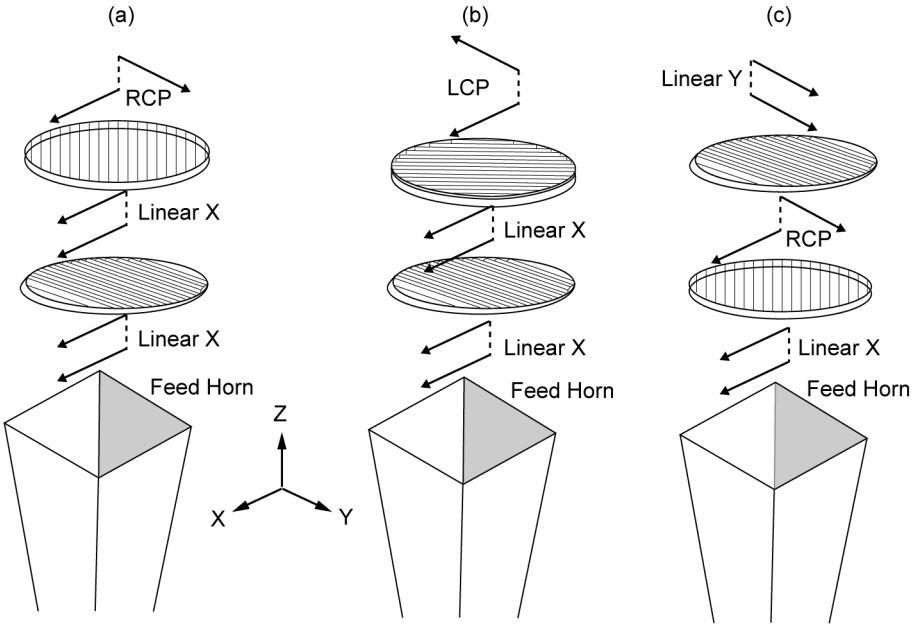

Fig. 9-21. Modes of operation of the dual-polarizer system: (a) right-hand circular polarization, (b) left-hand circular polarization, and (c) linear y.

design, development, testing, and performance of a phase-locked, two-element uplink array of 34-m-diameter BWG azimuth-elevation (az–el) radars operating at 7.19 GHz. The rms phase error of two coherent 100-ms, 50-pps (pulses per second), 5-kW peak pulses reflected from low Earth-orbiting debris with SNR > 23 dB is less than 4 deg, with monopulse pointing errors of less than 11-mdeg rms in winds up to 8.9 m/s (32.2 km/h). Each element has a radar SNR performance of 20.8 dB on a 0-dBsm target at 1000-km range. The elements are separated by 204 m on an east-west line at an altitude of approximately 1000 m at the Goldstone Deep Space Communications Complex in the Mojave Desert of California. Signal combination efficiencies approaching 98 percent have been achieved for tracks from 10-deg elevation at signal rise to 4-deg elevation at signal set. Acquisition and tracking are based upon orbital elements and the Simplified General Perturbations Model 4 (SGPM4), along with pointing calibrations based upon radio star and Defense Satellite Communications System (DSCS)-III racks. Both the 15-cm- (6-in.) and 10-cm- (4-in.) diameter spheres placed in orbit by the Space Transportation System (STS)-60 flight have been tracked.

9.6 Deep Space Station 27

When the ARST technology demonstration was completed, the antennas were turned over to the DSN to be used to track spacecraft. The first intended use was to track the SOHO (Solar and Heliospheric Observatory) spacecraft, which required one of the antennas—DSS-27—to be retrofitted with an S-band (2.2–2.3 GHz) feed system. Since the BWG optics was designed for 7.2 GHz, it was necessary to use a focal plane analysis method [10,11] to design the feed horn. The first step is to carry out a focal plane analysis of the antenna to compute a theoretical horn pattern (THP). The THP was then approximated by radiation patterns from corrugated horns. It was difficult to match the THP with corrugated feed-horn patterns, so several different cases were analyzed [12,13]. Ultimately, however, the aperture size was used that maximized gain and enabled the feed horn to be attached at the plate position that was built for the ARST primary feed system. The feed horn had a 24.8-dB gain at 2.295 GHz and was placed as shown in Fig. 9-22. The predicted S-band efficiency and noise-temperature performance are given in Tables 9-3 and 9-4. From Table 9-4 the predicted efficiency at 2.295 GHz referenced to the feed input is 49 percent.

The antenna efficiency was measured using the conventional three-point boresight technique on celestial radio sources [14]. The aperture efficiency at 2.29 GHz is 47 ± 2 percent at all elevation angles. These measurements are referenced to the low-noise-amplifier (LNA) input. The estimated uncertainty is

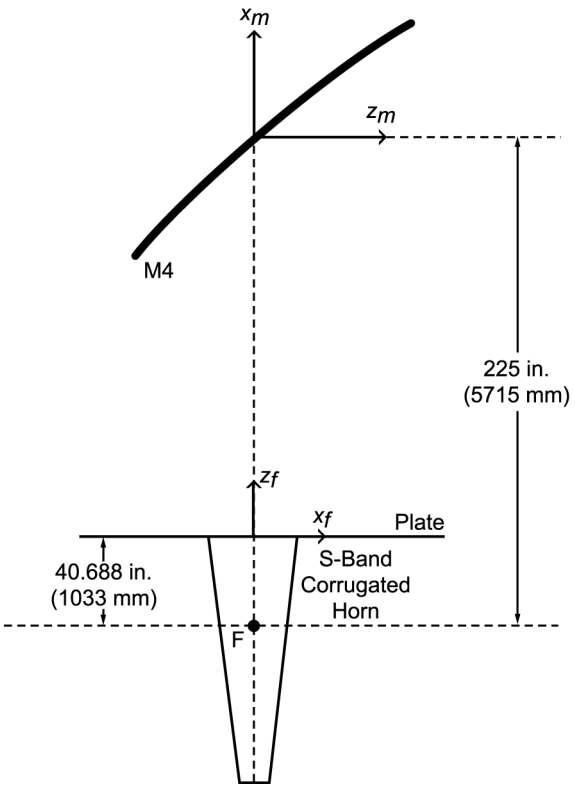

Fig. 9-22. S-band geometry.

2 percent. The data is corrected for atmospheric effects using a Goldstone standard atmosphere at 2.295 GHz of 0.03 dB.

The feed and waveguide loss must be subtracted from the efficiency measurements above to quantify the aperture efficiency of the antenna mechanical subsystem defined at the feed input. The feed and waveguide loss is estimated by converting the feed/waveguide noise temperature to loss at a physical temperature of 290 K.

The noise contribution of the feed horn (12.5 K) corresponds to a loss of 0.18 dB or 4.3 percent. The aperture efficiency referenced to the feed input is obtained by multiplying the efficiency referenced to the LNA input by this factor. This results in an efficiency referenced to the feed input of 49 ± 2 percent.

The individual components of the measured total system noise temperature at 2.290 GHz are shown in Table 9-5.

Table 9-3. S-band efficiency budget.

Element	Frequency (GHz)			Notes
	2.035	2.200	2.295	
Main reflector				
Ohmic loss	0.99976	0.99976	0.99976	Calculated
Panel leak	1	1	1	Calculated from DSS-24 model
Gap leak	1	1	1	Calculated from DSS-24 model
(Main reflector + subreflector) rms	0.99428	0.99428	0.99428	Calculated (rms = 0.20 mm)
Subreflector				
Ohmic loss	0.99976	0.99976	0.99976	Calculated
4 BWG Mirrors				
Ohmic loss	0.99903	0.99903	0.99903	Calculated
rms	0.99924	0.99924	0.99924	Calculated (rms = 0.20 mm)
BWG/Cassegrain VSWR	0.995	0.995	0.995	Estimated
Polarizer				
Ohmic loss	1	1	1	Removed from system
Reflection	1	1	1	Removed from system
Duplexing grid				
Ohmic loss	1	1	1	Removed from system
Reflection	1	1	1	Removed from system
Feed support blockage	0.9	0.9	0.9	DSS-24 model
Pointing squint	1	1	1	Removed from system
BWG mirror alignments	1	1	1	Unknown
Measurement uncertainty	0.9333	0.9333	0.9333	–0.3 dB
Subtotal	0.8291	0.8291	0.8291	Not applicable
Physical optics efficiency	0.5433	0.5722	0.5929	Physical optics analysis
Total at feed aperture	0.4505[a]	0.4744[b]	0.4916[c]	Not applicable

[a]57.21 dB = 100 percent; 53.75 dB = 45 percent.
[b]57.88 dB = 100 percent; 54.64 dB = 47.4 percent.
[c]58.25 dB = 100 percent; 55.17 dB = 49.1 percent.

Table 9-4. S-band noise-temperature budget.

Element	Frequency (GHz)			Notes
	2.035	2.200	2.295	
Main reflector				
Ohmic loss	0.07	0.07	0.07	Calculated
Panel leak	0.00	0.00	0.00	DSS-24 model
Gap leak	0.50	0.50	0.50	DSS-24 model
Rear spill	24.10	26.35	25.03	α = 240 K
Subreflector				
Ohmic loss	0.07	0.07	0.07	Calculated
Polarizer	0.00	0.00	0.00	Removed from system
Duplexing grid	0.00	0.00	0.00	Removed from system
Cosmic background	2.70	2.70	2.70	Effective blackbody
Atmosphere	1.80	1.80	1.80	Goldstone (average clear)
F_1 fields/forward spill/ ground	1.14	1.04	0.99	α = 5 K
4 upper BWG mirror spill	24.17	21.10	17.53	α = 180 K
4 BWG mirror ohmic loss	0.28	0.28	0.28	Calculated
Quadripod scatter	2.50	2.50	2.50	Estimated (DSS-24)
Subtotal (K)	61.33	56.41	51.48	Noise at feed aperture

Table 9-5. Measured noise temperature.

Noise-Temperature Component	T (K)	Notes
Sky	4.5	1.8-K atmosphere, 2.7-K cosmic background
Receiver	1.0	Measured
Low-noise amplifier	45.0	Measured
Feed/waveguide	12.5	From measurements of microwave system on ground
Antenna	40.1	Calculated by subtracting all the above from the total operating temperature
Total operating temperature	103.1	Total system-noise temperature

The noise contribution of the microwave subsystem is the sum of the LNA and the feed/waveguide contribution, or 57.5 K. The antenna mechanical subsystem contribution is 39.1 K. Observe that this temperature is lower than the 51.48 K given in Table 9-4. This is because the analysis used to compute the noise temperature did not include the effect of the BWG tube. A more accurate analysis based upon the techniques given in [15–17] yielded a more accurate estimate of 42.9 K.

The second antenna, DSS-28, has not been upgraded to include DSN frequencies and, for that reason, is currently not in use.

References

[1] H. Cooper, B. Conroy, J. Craft, R. Dickinson, D. Losh, and C. Yamamoto, *Antenna Research System Task Final Report*, JPL D-21208 (internal document), Jet Propulsion Laboratory, Pasadena, California, June 30, 1994.

[2] W. A. Imbriale, D. J. Hoppe, M. S. Esquivel, and B. L. Conroy, "A Beam-waveguide Design for High-Power Applications," *Intense Microwave and Particle Beams III*, proceedings of the SPIE conference, vol. 1629, Los Angeles, California, pp. 310–318, January 20–24, 1992.

[3] M. S. Esquivel, D. J. Hoppe, and W. A. Imbriale, *RF Design and Analysis of the ARST Antenna*, JPL D-11259 (internal document), Jet Propulsion Laboratory, Pasadena, California, November 1, 1993.

[4] M. Britcliffe, L. Alvarez, and M. Franco, "ARST Antenna RF Performance Measurements," JPL Interoffice Memorandum 3328-17-94 (internal document), Jet Propulsion Laboratory, Pasadena, California, March 4, 1994.

[5] S. B. Cohn, "Flare-Angle Changes in a Horn as a Means of Pattern Control," *The Microwave Journal*, pp. 41–46, October 1970.

[6] M. S. Esquivel, R. Frazer, D. J. Hoppe, F. Manshadi, R. Manvi, and H. Reilly, *ARST Primary Feed System Development*, JPL D-21209 (internal document), Jet Propulsion Laboratory, Pasadena, California, June 1994.

[7] K. R. Goudey and A. F. Sciambi, Jr., "High Power X-band Monopulse Tracking Feed for the Lincoln Laboratory Long-Range Imaging Radar," *IEEE Transactions on Microwave Theory and Techniques*, vol. MTT-26, no. 5, May 1978.

[8] J. R. Withington, W. A. Imbriale, and P. Withington, "The JPL Beam-waveguide Test Facility," *IEEE Antennas and Propagation Society Inter-*

national Symposium, vol. 2, Ontario, Canada, pp. 1194–1197, June 24–28, 1991.

[9] B. L. Conroy, D. J. Hoppe, and W. A. Imbriale, "Broadband Venetian Blind Polarizer with Dual Vanes," *International Journal of Infrared and Millimeter Waves*, vol. 14, no. 5, pp. 897–996, May 1993.

[10] W. A. Imbriale, "Design Techniques for Beam Waveguide Systems," *Proceedings of the International Conference on Millimeter and Submillimeter Waves and Applications III*, vol. 2842, Denver, Colorado, pp. 192–200, August 5–7, 1996.

[11] W. A. Imbriale, M. S. Esquivel, and F. Manshadi, "Novel Solutions to Low-Frequency Problems with Geometrically Designed Beam-Waveguide Systems," *IEEE Transactions on Antennas and Propagation*, vol. 46, no. 12, pp. 1790–1796, December 1998.

[12] M. S. Esquivel, "ARST 34-m BWG Antenna PO Analysis at S-band and X-band," JPL Interoffice Memorandum MSE-93-920 (internal document), Jet Propulsion Laboratory, Pasadena, California, October 14, 1993.

[13] M. S. Esquivel, "More S-band PO Analysis of DSS-27," JPL Interoffice Memorandum MSE-94-003 (internal document), Jet Propulsion Laboratory, Pasadena, California, January 2, 1994.

[14] M. J. Britcliffe, *DSS-27 Antenna RF Performance Measurements*, JPL D-12543 (internal document), Jet Propulsion Laboratory, Pasadena, California, March 15, 1995.

[15] A. G. Cha and W. A. Imbriale, "A New Analysis of Beam Waveguide Antennas Considering the Presence of the Metal Enclosure," *IEEE Transactions on Antennas and Propagation*, vol. 40, no. 9, pp. 1041–1046, September 1992.

[16] W. A. Imbriale, T. Y. Otoshi, and C. Yeh, "Power Loss for Multimode Waveguides and Its Application to Beam-Waveguide System," *IEEE Transactions on Microwave Theory and Techniques*, vol. 46, no. 5, pp. 523–529, May 1998.

[17] W. A. Imbriale, "On the Calculation of Noise Temperature in Beam Waveguide Systems," proceedings of the International Symposium on Antennas and Propagation, Chiba, Japan, pp. 77–80, September 24–27, 1996.